Journal of Solid State Chemistry **161,** 332–340 (2001)
doi:10.1006/jssc.2001.9322, available online at http://www.idealibrary.com on IDEAL®

Intercalation of Platinum Complex in LDH Compounds

P. Beaudot, M. E. De Roy,[1] and J. P. Besse

Laboratoire des Matériaux Inorganiques, Université Blaise Pascal, UMR CNRS 6002, 63177 Aubière Cedex, France

Received April 25, 2001; in revised form July 11, 2001; accepted July 23, 2001

Intercalation of platinum complex was carried out in [ZnAl], [MgAl], and [CuAl] LDH matrix by a new method including hydrothermal synthesis. Free carbonate products were obtained. XRD and FTIR studies show the total exchange. However, the geometry of the local environment of the platinum atom in the complex appeared to be modified during intercalation. By thermal treatments and reduction in ethylene glycol, metallic particles dispersed on oxide powder were obtained. The resulting calcined products could have some interest in heterogeneous catalysis. © 2001 Academic Press

Key Words: **LDH; platinum complex; dispersed metallic particles.**

INTRODUCTION

Layered double hydroxide (LDH) materials are the result of a combination of host structure resulting from the stacking of inorganic layers and chemical species trapped in the interlamellar domain. The structure looks like a brucite type with a 2D distribution of coplanar octaedra $[M(OH)_6]$ which corresponds to a hydrolyzed layer $M(OH)_2$ of the brucite.

The simultaneous presence of divalent and trivalent metallic cations in these layers leads to a positive charge which is balanced by anionic species trapped in the interlamellar space with water molecules. The ratio between divalent and trivalent metallic cations must be such that the $M^{III}/(M^{II} + M^{III})$ value is in the interval 0.2–0.4 for the majority of couples (M^{II}/M^{III}) (1). The general formula of LDH components is then $[M^{II}_{(1-x)}M^{III}_{(x)}(OH)_2]\ [X^{m-}_{x/m}\cdot nH_2O]$.

According to the fields of application, a great choice of metal composition (M^{II}/M^{III}) or interlayer species is possible. A main property of these materials is their anionic exchange capacity, which makes them unique inorganic materials for capture of organic and inorganic anions. It permits the use of LDH in several disciplines, such as medicine, environment, and, of course, catalysis (2–4). The purpose of this work is to replace anionic species like Cl^- and NO_3^- that are generally present in the interlamellar space by a metallic complex (5) to obtain materials that are active in heterogeneous catalysis. It is important to point out that many papers have already dealt with the subject and showed the interest of such compounds in heterogeneous catalysis (6). The ultimate aim is to prepare metallic nanoparticles on support oxide by using either thermal treatment or a direct reduction in ethylene glycol (7, 8). Nanoparticles with at least two metallic elements have recently appeared in the literature and seem interesting enough (9, 10). The choice of $[PtCl_6]^{2-}$ anion (11) as the complex to be trapped in the interlayer domain results in an important structural stability, which can offer really interesting possibilities for use of Pt metal in catalysis (12–19). In fact, we tried to obtain dispersed metallic nanoparticles using a method which differs from impregnation in order to use otherwise catalytic precursors. The synthesis of LDH containing noble metals, and particularly platinium, in the layers has been recently reported (20). However, difficulties in controlling and maintaining the $(Mg^{2+}–Pt^{2+}/Al^{3+})$ molar ratio appeared. Three different new LDHs intercalated with platinum complex were prepared. This allows us to have in the same compound three different metals. These products, noted in this publication [ZnAlPt] (platinum complex intercalated in ZnAl matrix), [MgAlPt] (platinum complex intercalated in MgAl matrix), and [CuAlPt] (platinum complex intercalated in CuAl matrix). This diversity of metals could give a large range of possibilities to create nanoparticles and might also give an interesting catalysis.

EXPERIMENTAL

Synthesis

$[ZnAlCl]_{LDH}$, $[MgAlCl]_{LDH}$, and $[CuAlCl]_{LDH}$ with ideal formulas $[Zn_2Al(OH)_6]Cl\cdot 2H_2O$, $[Mg_2Al(OH)_6]Cl\cdot 2H_2O$, and $[Cu_2Al(OH)_6]Cl\cdot 2H_2O$ were used as precursors for the studies of intercalation of $[PtCl_6]^{2-}$ anions in a LDH matrix.

Synthesis of precursors. These precursors were prepared by a coprecipitation method at controlled pH as described in the literature (21).

[1] To whom correspondence should be addressed. E-mail: Mariede_Roy@univ-bpclermont.fr.

0022-4596/01 $35.00

Respectively mixed solutions of $ZnCl_2$ (Prolabo)–$AlCl_3$ (Sigma, 99%), $MgCl_2$ (Sigma, 98%)–$AlCl_3$, and $CuCl_2$ (Prolabo, 99%)–$AlCl_3$ with the expected M^{II}/M^{III} ratio, having total cations concentrations equal to 1 M, have been used. The pH was maintained during coprecipitation at 8.5, 9.5, and 5.5, respectively, by simultaneous addition of 1 M NaOH to the mother solution. These syntheses were performed under a nitrogen atmosphere to prevent contamination by carbonate from atmospheric CO_2 at room temperature except for [MgAlCl] (65°C). We fixed the value of the molar ratio of M^{II}/M^{III} to 2, to create a higher positive charge for the layer, thus permitting a maximum of intercalation.

Anionic exchanges. The same method with little variation was used for the three precursors. The first step of the exchange was carried out at room temperature, under a nitrogen atmosphere, and with a K_2PtCl_6 (Strem, 99%) solution 4 times higher than the anionic capacity exchange of the LDH, for 90 min, 80 min, and 70 min for ZnAl, MgAl, and CuAl precursors, respectively.

In the second step, the three phases were introduced in an autoclave at 50°C under autogenous pressure of 1 kbar for 410 min and after that in an autoclave at 120°C under autogenous pressure of 2.4 kbar for 100 min, 90 min, and 70 min, respectively.

Powered products were recovered after quenching by centrifugation, three washing cycles with carbonate-free water being necessary. The powders were then dried at 50°C for 12 hours.

This method of synthesis was chosen because several attempts at using the methods commonly described, such as simple exchange, did not permit the intercalation of the complex.

Powder X-ray diffraction patterns were performed on a Siemens D 501 X-ray diffractometer using Cu$K\alpha$ radiation and fitted with a graphite scattered beam monochromator. The samples as unoriented powder were scanned from 2 to 76° (2θ) in steps of 0.08° with count time of 4 s at each point. Fourier transform infrared spectra were obtained, first with a Perkin Elmer 16PC spectrophotometer at a resolution of 2 cm^{-1} and avearing 10 scans in the 400–4000 cm^{-1} region on pressed KBr pellets, and second with a Perkin Elmer Parangon 1000 in CsI by diffuse reflectance, using a K.M. correction between 350 and 320 cm^{-1}.

Thermogravimetry was recorded on a Setaram TG DTA 92 thermogravimetric analyzer at a typical rate of 5°C min^{-1} under an air atmosphere. The nitrogen adsorption isotherms of the samples at liquid nitrogen temperature were recorded on a Coulter SA 100, inclulding prior pretreatment, which consisted of a degassing period of 500 min at 110°C. This was done to remove the adsorbed and interlayer water, and to leave only anions in the interlayer space. Pore distributions in all samples are calculated using the BJH model on the desorption branch. Elementary analyses were performed at the Vernaison Analysis Center of CNRS. Scanning electron micrographs were recorded at Technicauv S.A., France. Particle size distribution was determined on a Malvern Mastersizer 2000.

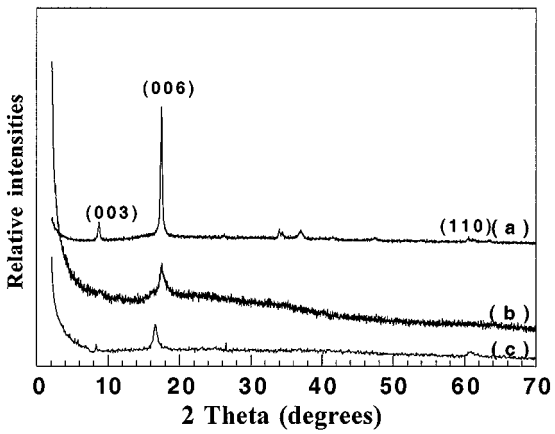

FIG. 1. Diffraction patterns of three LDH compounds intercalated with Pt complex in (a) [ZnAl], (b) [CuAl], and (c) [MgAl].

Zn K edge and Pt L_{III} edge. XAFS (X-ray absorption fine structure) studies were performed at LURE (Orsay, France) using X-ray synchrotron radiation emitted by the DCI storage ring (1.85 GeV positrons, average intensity of 250 mA) at the D44 line. Data were collected at room temperature in the transmission mode at the Zn K edge (9.658 eV) and the Pt L_{III} edge (11.563 eV). Three spectra were recorded for each sample. [ZnAlCl] and K_2PtCl_6 were taken as the reference materials; the theoretical functions from McKale's tables were taken as the phase and amplitude (22). The EXAFS signal treatments and refinements were performed with the program package developed by A. Mickalowicz (23). The commonly accepted accuracy of the fit is about 0.02 Å for the distance and 10 to 20% for the number of neighbors. The module of the Fourier transform corresponds to the pseudo radial distribution functions (pseudo RDF).

TABLE 1
Indexation of [ZnAlPt] in *R*-3*m* Space Group

(*hkl*)	(003)	(006)	(009)	(010)	(012)	(015)	(0014)	(018)	(0111)	(110)	(112)
2θ (degrees)	8.32	17.20	26.04	33.96	36.98	41.51	46.04	47.35	51.88	60.45	61.88

TABLE 2
Interlayer Distances of Precursors and Intercalated Products

Sample	[ZnAlCl]	[ZnAlPt]	[MgAlCl]	[MgAlPt]	[CuAlCl]	[CuAlPt]
Interlayer distance (Å)	7.99	10.13	7.96	10.73	7.81	10.08

RESULTS AND DISCUSSION

The completeness of exchange of chloride by the anionic complex was confirmed by chemical analysis and X-ray powder diffraction.

X-ray powder diffraction patterns of exchanged products are presented in Fig. 1. The [ZnAlPt] sample gives the best PXRD pattern. In [MgAlPt] and [CuAlPt], we can observe an important amorphous phase. However, there is no remaining crystallized LDH chloride precursors. The PXRD general aspect evidences that all the samples are hardly well ordered.

The diffraction peaks are indexed using a hexagonal cell with rhombohedral symmetry ($R\bar{3}m$) (Table 1) where the c parameter corresponds to 3 times the interlamellar distance d (003) and the a parameter which represents the average intermetallic distance is calculated from the position of the d (110) ray. For [ZnAlPt] and [MgAlPt] the calculated parameters are $a = 3.06(3)$ Å, $c = 30.3(9)$ Å and $a = 3.05(2)$ Å, $c = 32.7(9)$ Å, respectively. Interlayer distances in precursors and in exchanged products are compared in Table 2.

For the three compounds, we observed an inversion of intensity of the first two (001) peaks in intercalated products, compared to the LDH chloride precursors (Fig. 2). This phenomenon appeared in previous work on LDHs containing heavy interlayer molecular species such as chromate or vanadate in a [MgAl] matrix (21, 24) and oxalate in a [ZnAl] matrix (25).

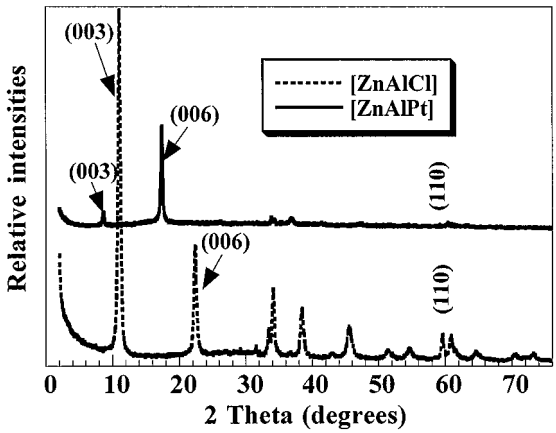

FIG. 2. Comparison of the diffraction patterns of [ZnAlPt] and [ZnAlCl] compounds.

A common feature of all the X-ray patterns is that the second (001) diffraction line becomes more accentuated than the first one. This has been attributed to the increase in electron density in the midplane of the interlayers due to the presence of the heavy metal. In this case, the XRD patterns show an important intensity ratio between (003) and (006) diffraction lines, which could be linked to the important electronic density of Pt.

In the precursor, the position commonly assigned to the Cl^- anion is the 18g site of the $R\bar{3}m$ space group (26). If we use the position with $z = 1/2$ for the Pt atom in the exchanged product, the ratio between the diffusion atomic factor of Pt and Cl^- is around 5.13 for the (003) and (006) diffraction lines.

This would explain the inversion observed in the relative intensities of (003) and (006) diffraction lines between the precursor containing Cl^- anions and the exchanged phase containing Pt complex within the layers.

This phenomenon clearly points out the presence of a heavy atom between the layers.

TABLE 3
Chemical Formula of Intercalated Products

Sample	Formula[a]	Cl/Pt[b]	M^{II}/M^{III} [b]	
			In intercalated products	In precursor
[ZnAlPt] (%)	$[Zn_{0.59}Al_{0.39}(OH)_2][Pt(Cl_{3.2}(OH)_{2.8})]_{0.17}$,1.81 H_2O Zn, 19.81; Al, 5.36; Pt, 17.23; Cl, 9.82; H, 3.13	3.2	1.51	1.98
[MgAlPt] (%)	$[Mg_{0.63}Al_{0.35}(OH)_2][Pt(Cl_{3.6}(OH)_{2.4}]_{0.16}$.1.64 H_2O Mg, 10.63; Al, 6.64; Pt, 21.61; Cl, 14.12; H, 3.93	3.6	1.79	2.06
[CuAlPt] (%)	$[Cu_{0.61}Al_{0.36}(OH)_2[Pt(Cl_{2.4}(OH)_{3.6}]_{0.16}$.0.68 H_2O Cu, 23.52; Cu, 23.52; Al, 5.95; Pt, 19.06; Cl, 8.41; H, 2.38	2.4	1.69	2.04

[a] Figures have been rounded to two digits. [b] Molar ratio.

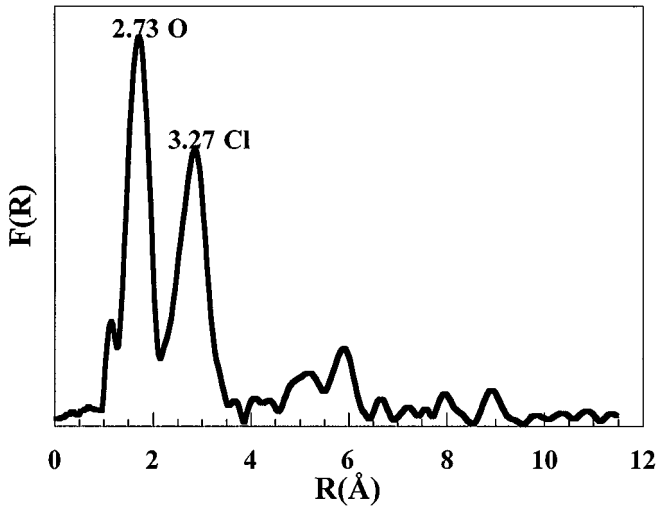

FIG. 3. Fourier transform of Pt neighbors in [ZnAlPt] at the Pt L_{III} edge.

Chemical compositions of obtained compounds are reported in Table 3. In all cases, the chloride content is lower than expected, while the hydroxyl group content is higher. We have not found in the literature work which reports the study of the complex evolution during the exchange in LDH phases. But, progressive hydrolyzation of K_2PtCl_6 to $K_2Pt(OH)_6$ is relatively well known (27–30), which leads to intermediate compounds $K_2Pt(OH)_5Cl$, $K_2Pt(OH)_4Cl_2$, $K_2Pt(OH)_2Cl_4$, and $K_2Pt(OH)Cl_5$. The Cl/Pt molar ratio appeared different in the three matrixes. It seems that it is not the same platinum complex which is intercalated in the different matrix. But we noted also a slight decrease in the M^{II}/M^{III} molar ratio which could be explained by a partial dissolution of the divalent ion of the layers or a dissolution–

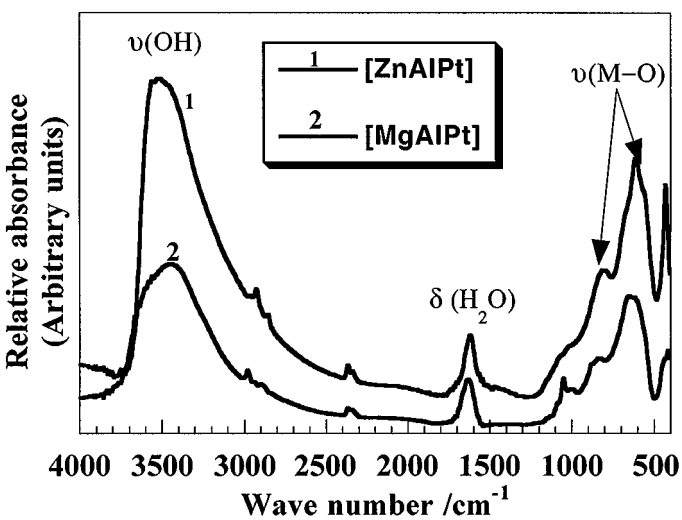

FIG. 4. Infrared spectra of [ZnAlPt] and [MgAlPt] between 4000 cm^{-1} and 400 cm^{-1}.

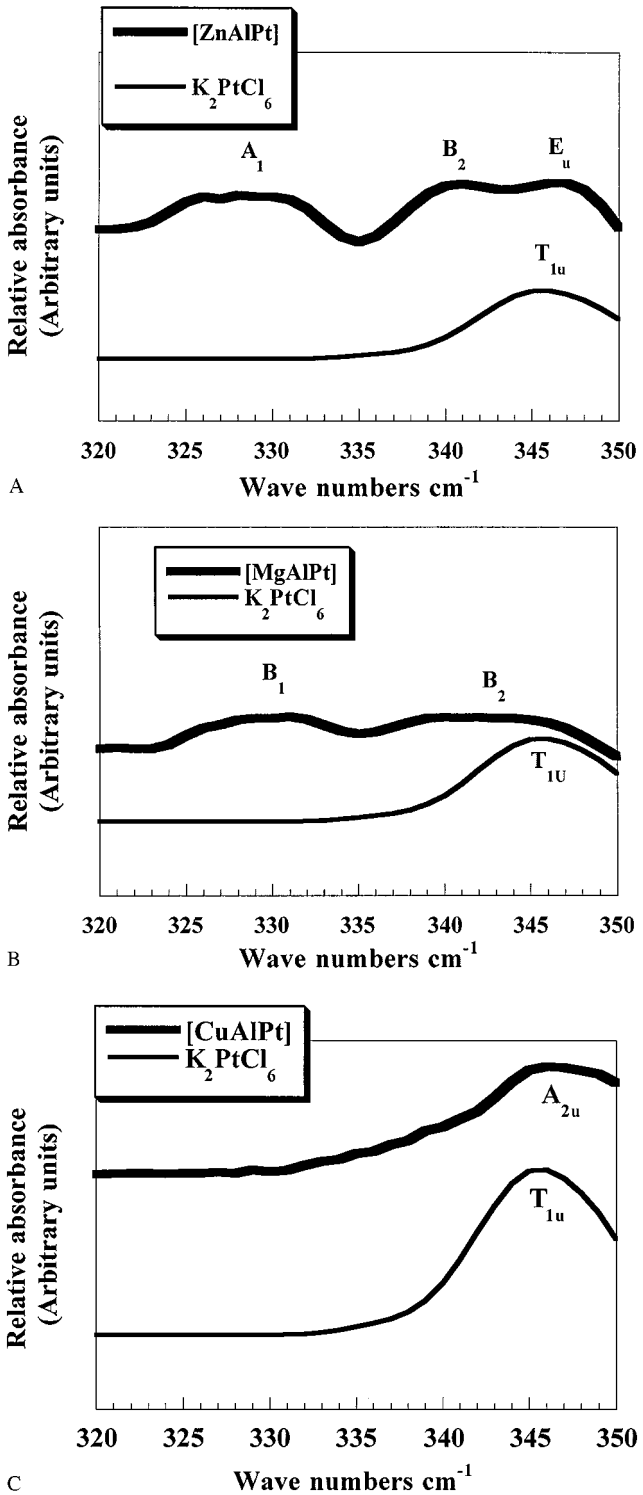

FIG. 5. Infrared spectra of [ZnAlPt] and K_2PtCl_6 (A), [MgAlPt] and K_2PtCl_6 (B), and [CuAlPt] and K_2PtCl_6 (C) between 350 cm^{-1} and 320 cm^{-1}.

reconstruction due to hydrothermal synthesis and acidic domain the $[PtCl_6]^{2-}$ anion (from pH 2 to 5.5) (19). The existence of defective sheets has already been noted for

TABLE 4
Parameters of EXAFS Study at Pt L_{III} Edge

Sample	N_1	R_1	$\sigma_1 = \sigma_2$	$\Gamma_1 = \Gamma_2$	N_2	R_2	Residue
[ZnAlPt]	2.73	1.99	0.0594	0.807	3.27	2.32	8.5×10^{-3}

σ_i, Debye–Waller factor; N_i, effective coordination number; R_i, interatomic distance between studied atom and its neighbors (Å); Γ_i, factor related to the mean free path λ of the photoelectron ($\lambda = k/\Gamma$); Residue, disagreement factor.

tetracyanoquinodimethane (31) and $RuCl_5H_2O$ (32) in [ZnAl] matrix and reported for the synthesis of pillared clays with Keggin ions (33). An EXAFS study was conducted in order to confirm or repute these results.

X-Ray Absorption Spectroscopy

X-ray absorption spectra were obtained at the Zn K edge for [ZnAlCl] and [ZnAlPt] and at the Pt L_{III} edge for K_2PtCl_6 and [ZnAlPt].

The study at the Zn K edge shows that the two pseudo radial distribution functions are superimposed so that we can conclude that the local order around the Zn atom in the layers remains identical after exchange with the platinium complex.

As to the reference compound K_2PtCl_6, the study at the Pt L_{III} edge gives results corresponding to the well-known octahedral environment of the $[PtCl_6]^{2-}$ anion (11). For the exchange compound [ZnAlPt], the parameters of refinement of the first shell around the platinum atom, which contains only a single scattering contribution, are reported in Table 4. The results show a strongly distorted and mixed environment around the platinum atom: 3.27 chloride atoms at 2.32 Å (11) and 2.73 oxygen atoms at 1.99 Å (around Pt–O distance in $[Pt(OD)_6]^{2-}$ anion 2.06(2) Å (34)) (Fig. 3). These values represent an average of local environment of Pt atoms. These data correspond to the chemical composition of [ZnAlPt].

IR Spectroscopy

The characteristic bands reported in the literature for the anion $[PtCl_6]^{2-}$ are located at frequencies lower than 400 cm^{-1} (35), so the IR study was performed first between 4000 and 400 cm^{-1} with KBr pellet method and then in CsI by diffuse reflectance between 350 and 320 cm^{-1}.

With the first study we could note that the IR spectra shown in Fig. 4 correspond to compounds free of carbonate contamination. The main absorption band centered at 3477 cm^{-1} corresponds to the vibration ν(OH) of the hydroxyl group forming the brucite-like layers as well as the interlamellar water. The other intense band at 1600 cm^{-1} is normally assigned to the vibration resulting from the water molecule $\delta(H_2O)$. The bands appearing at frequencies lower than 800 cm^{-1} correspond to the metal–oxygen vibration δ(M–OH). Bands at 2985 and 2901 cm^{-1}, which appear in the exchange products, are characteristic of hydrocarbon contamination.

The higher crystallinity of the host network of [ZnAlPt] is evidenced by the high resolution of the lattice vibration, which appears in the wavenumber range (400–650 cm^{-1}). The IR spectra between 400 and 4000 cm^{-1} are typical of LDH.

The comparison of infrared spectra curves (which are all on the same scale) of K_2PtCl_6, [ZnAlPt], [MgAlPt], and [CuAlPt], obtained between 350 and 320 cm^{-1}, is shown in Figs. 5A, 5B, and 5C. For [ZnAlPt], the bands may be tentatively attributed to the IR-active band E_u which corresponds to a trans $[PtCl_4(OH)_2]^{2-}$ and to IR-active bands B_2–A_1 which correspond to trans $[PtCl_3(OH)_3]^{2-}$ (29, 30). We could then obtain a mixture of the two compounds. For [MgAlPt], the bands may be tentatively attributed to IR-active bands B_1–B_2 which correspond to a cis $[PtCl_4$

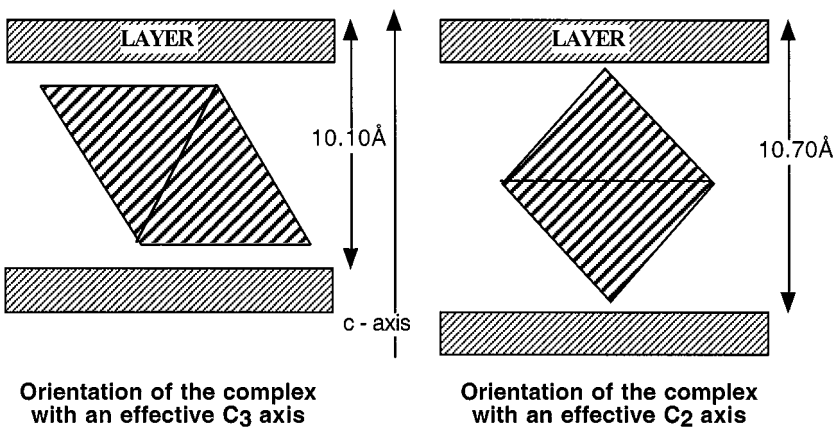

FIG. 6. Possible orientations of the complex between the layers.

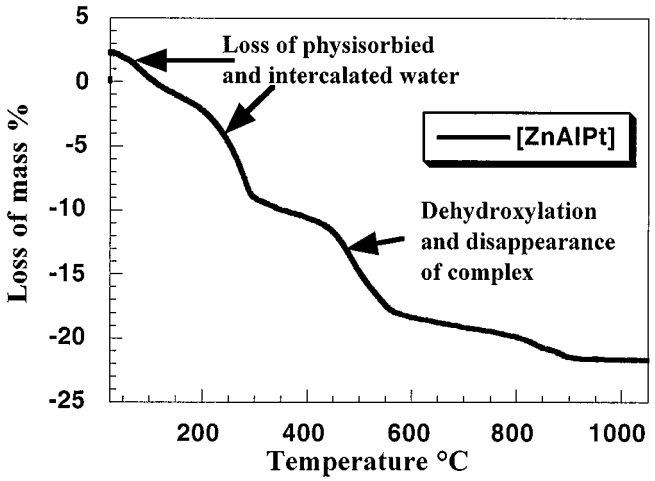

FIG. 7. TG data of [ZnAlPt].

$(OH)_2]^{2-}$. For [CuAlPt], the band may be tentatively attributed to the IR-active band A_{2u} which corresponds to a trans $[PtCl_2(OH)_4]^{2-}$.

As was shown by the study on XRD, the platinum atom is present between the ZnAl layers and is surrounded by both chloride and oxygen atoms, forming a distorted octahedral environment. So the species observed in the interlamellar domain after exchange could be the mixed-ligand species $[PtCl_{(6-x)}(OH)_x]^{2-}$.

Investigations on the intercalation of metal complexes into LDH have shown that guest–host interactions can affect the orientation and stability of intercalated complexes (36, 37). The metallic complex of platinum within the hydrotalcite layers can intercalate in two different orientations, which correspond to different basal spacing of 10.13 and 10.08 Å, respectively. [ZnAlPt] and [CuAlPt] with the effective C_3 axis are perpendicular to the brucite-like layers and aligned along the z axis and 10.73 Å, while [MgAlPt] with the effective C_2 axis of the pseudo octahedral anion is perpendicular to the brucite-like layers and aligned along the z axis (Fig. 6).

These two different possibilities of orientation could explain the difference in basal spacing observed between [ZnAlPt], [CuAlPt], and [MgAlPt]. It could be due to a more important basicity in the [MgAlPt] phase resulting from the higher value of pH during the precipitation of precursor. The basicity which is inversely connected to electronegativity (1.2, 1.65, and 1.9 for Mg, Zn, and Cu, respectively) could create more interactions between hydroxyl groups and the layers.

TG Data

The thermal decompositions of [ZnAlPt] (Fig. 7), [MgAlPt], and [CuAlPt] are rather similar, and correspond to chemical compositions. The desorption of adsorbed water is complete around 120°C while the desorption of structural water molecules occurs at higher temperatures and is complete at 230°C. The next step consists of

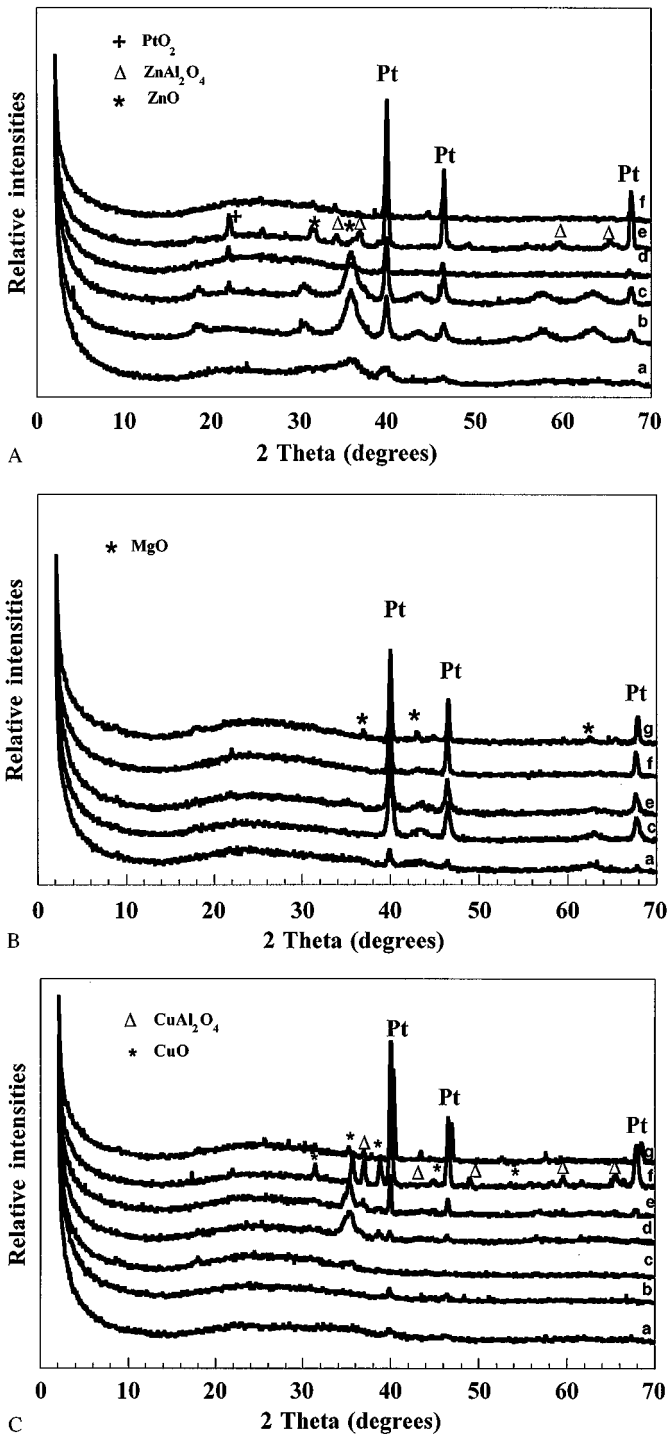

FIG. 8. Diffraction patterns of [ZnAlPt] (A), [MgAlPt] (B), and [CuAlPt] (C) calcined respectively at (a) 400°C, (b) 500°C, (c) 600°C, (d) 700°C, (e) 800°C, (f) 900°C, and (g) 1050°C. The diffraction rays which appear at high temperature correspond to oxide or mixed oxide.

TABLE 5
Thermal Evolution of Intercalated Products[a]

Compound	400°C	500°C	600°C	700°C	800°C	900°C	1050°C
[ZnAlPt]	Am.Ph.–ZnO	Am.Ph.–ZnO	ZnO–Pt	ZnO–PtO_2–Pt	ZnO–PtO_2–Pt	ZnO–$ZnAl_2O_4$–PtO_2–Pt	$ZnAl_2O_4$–Pt
[MgAlPt]	Am.Ph.–MgO–Pt		Am.Ph.–MgO–Pt		Am.Ph.–MgO–Pt	Am.Ph.–MgO–Pt	Am.Ph.–MgO–Pt
[CuAlPt]	Am.Ph.	Am.Ph.	Am.Ph.	CuO–$CuAl_2O_4$–Pt	CuO–$CuAl_2O_4$–Pt	CuO–$CuAl_2O_4$–Pt	Am.Ph.–Pt

[a] Am.Ph, amorphous phase.

simultaneous loss of water molecules resulting from hydroxyl groups' decomposition and chloride anions coming from the platinum complex. These two decompositions are not separated precisely but it is obvious that the deshydroxylation occurs at lower temperature than the decomposition of intercalated anion (38). The end of complex decomposition occurs around 820°C.

The study was completed by XRD analysis of samples heated at different temperatures from 400°C to 1050°C. The patterns of [ZnAlPt], [MgAlPt], and [CuAlPt] are shown in Figs. 8A, 8B, and 8C.

For [ZnAlPt] and [CuAlPt] three stages are observed as the temperature increases: first the amorphization of LDH material followed by the appearance of metallic oxide and mixed metallic oxide. The crystallinity of these oxides decreases at high temperature while metallic platinum is formed.

We can note that the diffraction lines of metallic platinium appear at a lower temperature for [MgAlPt] (400°C) than for the other compounds, so it seems that more Cl^- anions could lead to an earlier appearance of metallic platinum. For the $[(Mg–Pt)/AlCO_3]_{LDH}$ phase, Basile *et al.* (20) indicated the appearance of metallic platinum around 650°C. At a temperature higher than 700°C the three calcined phases are characterized by the coexistence of metallic platinum and amorphous metallic oxides.

The different phases and temperature domains observed are reported in Table 5 for the three compounds.

Presented in Table 6 is the size of crystallites obtained by the law of Debye–Sherrer applied to the (111) ray of metallic platinum for [ZnAlPt] during a thermal evolution.

Another way to obtain metallic platinum dispersed in an inorganic matrix is to submit the intercalated LDH to a reducer treatment. With this aim, we obtained the compound [ZnAlPt] under refluxing ethylene glycol over 3 weeks under a nitrogen atmosphere with polyvinylpyrrolidone as catalyst (8).

TABLE 6
Size of [ZnAlPt] Crystallites during a Thermal Evolution from the Platinum Ray (111)

Temperature	600°C	700°C	800°C	900°C	1050°C
Size Å	742	788	1242	1492	1688

The X-ray diffractogram of this resulting product is presented in Fig. 9. The diffraction lines of metallic platinum are smaller and broader than these observed for calcined phases.

It seems that, in this case, the metallic platinum is more dispersed in the midst of amorphous oxide phase; this could lead to a possible catalytic application.

Some phases have been observed by scanning electron microscopy. At room temperature [ZnAlPt] has no "sand rose" morphology observed in [ZnAlCl] (25), but appears as hexagonal plates which are dispersed. It is probably the effect of the hydrothermal part of synthesis (pressure). Calcined phases at 400°C showed large crystallites of ZnO with small attached spherical particles of $ZnAl_2O_4$. Calcined phases at 900°C present a porous aspect (Fig. 10).

In order to get the most information on [ZnAlPt] compounds, we performed a granulometric study at room temperature, where we noted an average particle size distribution of 19.5 μm. To complete these data, we have calculated the coherence length along c: L_c, by the Debye–Sherrer law (39). L_c of [ZnAlPt], [MgAlPt], and [CuAlPt]

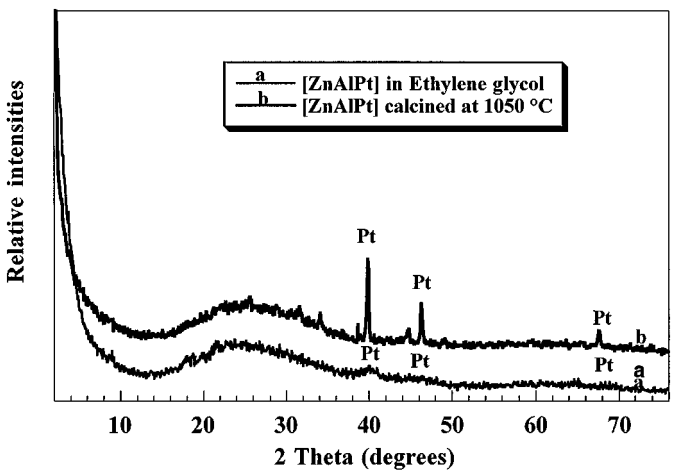

FIG. 9. Comparison of diffraction patterns of [ZnAlPt] calcined at 1050°C and [ZnAlPt] treated in ethylene glycol.

compounds have been calculated from the (003) and (006) planes employing the Debye–Sherrer equation $t = 0.9\lambda/(\beta \cos \theta)$, where t is the crystallite size (for us L_c), λ is the wavelength of the radiation used, β is the full width at half-maximum (FWHM) in radians (we subtracted the experimental width obtained with a silica spectrum), and θ is the Bragg diffraction angle; the values are 422 Å, 267 Å, and 251 Å, respectively, for [ZnAlPt], [MgAlPt], and [CuAlPt].

Specific Surface Area

Synthetic LDH compounds are widely used as precursors for the preparation of mixed oxide catalyst (40). We carried out a systematic analysis of the nitrogen adsorption/desorption of the LDH intercalated with platinum oxide. These macroscopic properties can be directly related to the inner structure of the material and to its morphology. The N_2 adsorption/desorption curves of compounds at room temperature (Fig. 11) are typical of mesoporous materials. A similar behavior was described for LDH reference materials such as [ZnAl] and [MgAl] containing chloride or carbonate (41). In most cases, the exchange of chloride anions by platinum complex have no significant effect on the surface area (from 44 to 32.9 m^2/g for [MgAlPt] and from 25 to 42 m^2/g for [ZnAlPt]). This could be due to a compact arrangement of anions. This was already observed with the oxo-anions (42).

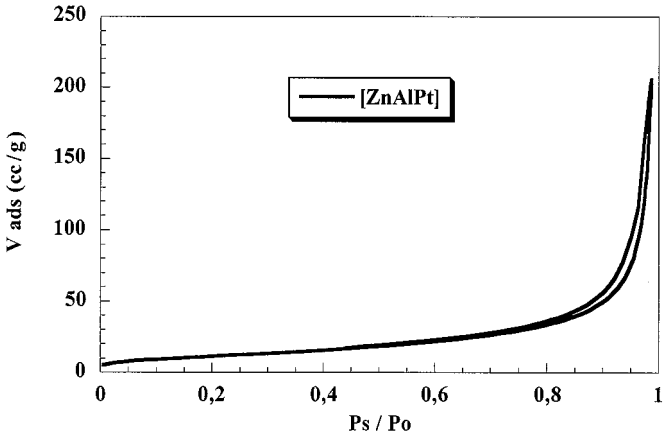

FIG. 11. N_2 adsorption/desorption isotherms of [ZnAlPt] of noncalcined phases.

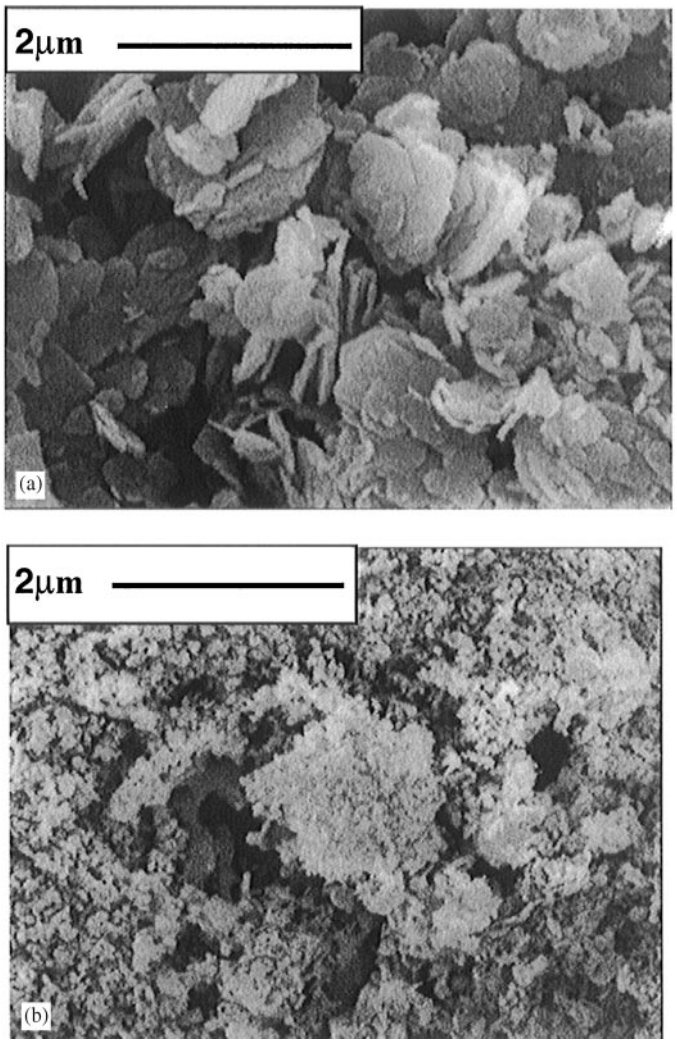

FIG. 10. SEM of [ZnAlPt] at room temperature (a) and calcined at 900°C (b).

In calcined phases [ZnAlPt] and [CuAlPt] (400°C), we observed decreases or no significant variations as a result of the thermal treatment. The specific surface areas are low as for the chloride precursors, but mesoporous structure is also preserved. An explanation was given to account for this phenomena (43); it consists of rapid dehydration followed by rapid crystallization of metal oxides. The specific surface areas of [MgAlPt] at 420°C and [ZnAlPt] at 510°C, just after the appearance of metallic particles platinum, are respectively 83 m^2/g and 69 m^2/g. These values are interesting. For [MgAlPt] specific surface areas are 89 m^2/g at 470°C, 107 m^2/g at 620°C, and 86 m^2/g at 890°C. At these temperatures we did not observe an important decrease in the specific surface area, in contrast to the results of Basile *et al.* (20) describing LDH with platinum in the layers (197 m^2/g at 650°C and 55 m^2/g at 900°C). The authors think that the presence of segregated side phases (such as metallic platinum, which is observed at this temperature) decreases the surface areas, probably by occlusion of the smallest pores and/or structural rearrangement. So, with an intercalation of platinum complex method, we have at lower temperature smaller but constant specific surface areas than for LDH with platinum in the layer (20).

CONCLUSION

The study, carried out on the intercalation of platinum complex in LDH, shows the reality of this intercalation by XRD and FTIR spectoscopy. But, we can note amorphous phases in [MgAlPt] and [CuAlPt]. A total exchange occurred without carbonate impurities. However, elementary analysis revealed an evolution of the complex composition with the loss of Cl^- anions; this result could be linked to the modification of the geometrical environment of the Pt atom observed in the XAFS study. The best hypothesis is the progressive hydrolization of the complex, hydroxyl group by hydroxyl group. We noted differences in the loss of Cl^- anion in the three products, so we saw the importance of the metallic components of the matrix. The evolution of the interlayer distances in the three products was probably due to the differences in basicity which determine the amount of hydroxyl group replacing Cl^- in the pseudo octahedral anion. Specific surface areas obtained after thermal treatment seem to be interesting, but the important fact is the appearance of metallic particles of platinum in mixed oxides support obtained on calcined phases and on phases treated in ethylene glycol. The relatively good dispersion could permit a use in catalysis (tests on [MgAlPt] are in progress).

ACKNOWLEDGMENTS

We acknowledge Mrs. A. M. Gelinaud who carried out scanning electron micrograph studies. We thank too the LURE, Mr. A. de Roy, and Mr. F. Leroux for allowing us access to the EXAFS facility and Mrs. P. Ceysset and Mrs. A. Henderson as translators for helpful discussions.

REFERENCES

1. S. Miyata, *Clays Clay Miner.* **28,** 50 (1980).
2. A. de Roy, C. Forano, K. el Malki, and J. P. Besse, in "Anionic Clays: Trends in Pillaring Chemistry" (Ocelli and Robson, Eds.), Vol. II, Chap. 7, p. 108. Van Nostrand Reinhold, New York, 1992.
3. A. Vaccari, *Appl. Clay Sci.* **14,** 161 (1999).
4. I. Rousselot, C. Taviot-Guého, and J. P. Besse, *Int. J. Inorg. Mater.* **1,** 165 (1999).
5. V. Rives and M. A. Ulibarri, *Coord. Chem. Rev.* **181,** 61 (1999).
6. F. Cavani, F. Trifiro, and A. Vaccari, *Catal. Today* **11,** 173 (1991).
7. M. S. Hedge, D. Larcher, L. Dupont, B. Beaudoin, and J. M. Tarascon, *Solid State Ionics* **93,** 33 (1997).
8. F. Kooli, V. Rives, and W. Jones, *Chem. Mater.* **9,** 2231 (1997).
9. M. Freemantle, *Chem. Eng. News* October 12, 40 (1998).
10. R. V. Malyala, C. V. Rode, M Arai, S. G. Hedge, and R. V. Chaudhari, *Appl. Catal. A: General* **193,** 71 (2000).
11. R. W. G. Wyckoff, "Crystal Structures," Vol. 3, 2nd Ed. Wiley, New York, 1965.
12. Z. Gandao, B. Coq, L. C. de Ménorval, and D. Tichit, *Appl. Catal. A: General* **147,** 395 (1996).
13. M. Spiro and A. B. Ravnö, *J. Chem. Soc.* 78 (1965).
14. M. Spiro and A. B. Ravnö, *J. Chem. Soc.* 97 (1965).
15. B. Shelimov, J. F. Lambert, M. Che, and B. Didillon, *J. Am. Chem. Soc.* **121,** 545 (1999).
16. B. Shelimov, J. F. Lambert, M. Che, and B. Didillon, *J. Catal.* **185,** 462 (1999).
17. J. R. Regalbuto, A. Navada, S. Shalid, M. L. Bricker, and Q. Chen, *J. Catal.* **184,** 335 (1999).
18. T. V. Kireeva, V. P. Doronin, L. Ya. Alt, and V. K. Duplyakin, *React. Kinet. Catal. Lett.* **34,** 261 (1987).
19. T. Mang, B. Breitscheidel, P. Polanek, and H. Knözinger, *Appl. Catal. A: General* **106,** 239 (1993).
20. F. Basile, G. Fornasari, M. Gazzano, and A. Vaccari, *Appl. Clay Sci.* **16,** 185 (2000).
21. S. Miyata, *Clays Clay Miner.* **31,** 305 (1983).
22. A. G. Mac Kale, B. W. Veal, A. P. Paulikas, S. K. Chan, and J. Knapp, *J. Am. Chem. Soc.* **110,** 3763 (1988).
23. A. Mickalowicz, Programs available on the web site of lure: http://www.lure.fr.
24. F. Malherbe, Synthèse, caractérisation et application en catalyse hétérogene de matériaux lamellaires de type hydrotalcite, Ph.D thesis, Université de Clermont-Ferrand, France, 1997.
25. V. Prevot, C. Forano, and J. P. Besse, *J. Mater Chem.* **9,** 155 (1999).
26. H. Roussel, V. Briois, E. Elkaim, A. de Roy, and J. P. Besse, *J. Phys. Chem. B* **104,** 5915 (2000).
27. P. Pascal, "Nouveau traité de chimie minérale." Vol. 19. p. 664, Masson, Paris, 1958.
28. C. Carr, P. L. Goggin, and R. J. Goodfellow, *Inorg. Chim. Acta.* **81,** 25 (1984).
29. P. Erlhöfer and W. Preetz, *Z. Naturforsh.* **44b,** 619 (1989).
30. W. Preetz and G. Rimkus, *Z. Naturforsh.* **37b,** 579 (1982).
31. S. Bonnet, C. Forano, and J. P. Besse, *Mater. Res. Bull.* **33,** 783 (1998).
32. J. Inacio, C. Taviot-Guého, S. Morlat-Thérias, M. E. de Roy, and J. P. Besse, *J. Mater. Chem.* **11,** 640 (2001).
33. J. Wang, Y. Tian, R. C. Wang, and A. Clearfield, *Chem. Mater.* **4,** 1276 (1992).
34. G. Bandel, Müllner, and M. Trömel, *Z. Anorg. Allg. Chem.* **453,** 5 (1979).
35. K. Nakamoto, "Infrared and raman spectra of inorganic and coordination compounds." Wiley, New York, 1997.
36. F. Kooli, I. C. Chisem, M. Vucelic, and W. Jones, *Chem. Mater.* **8,** 1962 (1996).
37. N. H. Gutmann, L. Spiccia, and T. W. Turney, *J. Mater. Chem.* **10,** 1219 (2000).
38. A. de Roy, A. M. Vernay, J. P. Besse, and G. Thomas, *Analusis* **16**(7), 409 (1988).
39. B. D. Cullity, "Elements of X ray diffraction," Addition-Wesley, Reading, MA, 1959.
40. A. Vaccari, "Synthesis and applications of anionic clays." Elsevier, Amsterdam, 1995.
41. F. Malherbe, C. Forano, and J. P. Besse, *Microporous Mater.* **10,** 67 (1997).
42. F. Malherbe, C. Depège, C. Forano, J. P. Besse, M. P. Atkins, B. Sharma, and S. R. Wade, *Appl. Clay Sci.* **13,** 451 (1998).
43. V. Prevot, C. Forano, and J. P. Besse, *Inorg. Chem.* **37,** 4293 (1998).